

ISMIP6 future projections for the Greenland ice sheet with the model SICOPOLIS

Ralf GREVE^{1,2}, Christopher CHAMBERS¹, Reinhard CALOV³

¹Institute of Low Temperature Science, Hokkaido University,
Sapporo, Japan

²Arctic Research Center, Hokkaido University, Sapporo, Japan

³Potsdam Institute for Climate Impact Research, Potsdam, Germany

Contact: R. Greve (greve@lowtem.hokudai.ac.jp)

September 17, 2020

Abstract

The Ice Sheet Model Intercomparison Project for CMIP6 (ISMIP6) brings together a consortium of international ice-sheet and climate modellers to simulate the contribution from the Greenland and Antarctic ice sheets to future sea-level rise. In this document (supplementary to Goelzer et al. 2020, doi: 10.5194/tc-14-3071-2020), we describe the ISMIP6 Greenland Tier-1 and Tier-2 experiments carried out with the ice-sheet model SICOPOLIS. First, we conduct a paleoclimatic spin-up over the last glacial-interglacial cycle until the year 1990. In this spin-up, we employ a nudging technique for the topography and aim at optimizing the match between simulated and observed surface velocities by adjusting the amount of basal sliding for individual drainage systems. Then, we carry out a historical run to bridge the gap between 1990 and 2015. The future climate projections run from the beginning of 2015 until the end of 2100. The simulated mass loss by 2100 is 133.0 ± 40.7 mm SLE (mean \pm 1-sigma uncertainty; SLE: sea-level equivalent) for the RCP8.5/SSP5-8.5 pathway that represents “business as usual”, and it is 48.6 ± 6.2 mm SLE for the RCP2.6/SSP1-2.6 pathway that represents substantial emissions reductions. The large difference between the results for the two pathways highlights the importance of efficient climate change mitigation for limiting sea-level rise. Further, results obtained with forcings from the newer CMIP6 global climate models consistently produce larger mass losses than those obtained with the older CMIP5 global climate models.

1 Introduction

The Coupled Model Intercomparison Project Phase 6 (CMIP6) is a major international climate modelling initiative (Eyring et al. 2016). As a part of this project, the Ice Sheet Model Intercomparison Project for CMIP6 (ISMIP6) was devised to assess the likely sea-level-rise contribution from the Greenland and Antarctic ice sheets until the end of this century (Nowicki et al. 2016, 2020).

Goelzer et al. (2020) describe the set-up and results of the ISMIP6 projections for the Greenland ice sheet. The ensemble of simulations is based on 21 sets of ice-flow simulations from 14 modelling groups. The design of the experiments is sketched in Fig. 1. An initial state of the ice sheet is produced by either assimilation or spin-up techniques or a combination of both (Goelzer et al. 2018, Seroussi et al. 2019). The initialization date varies between the different models (here 1990 CE). A single historical run with a forcing that can be chosen freely bridges the gap between the initialization and the start date of the projections in January 2015. All projections run from this date until December 2100. The atmospheric forcing consists of anomalies for the surface mass balance (SMB) and surface temperature (ST), derived from selected CMIP5 and CMIP6 global climate models (Barthel et al. 2020) and then downscaled to the surface of the ice sheet by the regional climate model MAR (Modèle Atmosphérique Régional) v3.9.6 (Fettweis et al. 2017, Delhasse et al. 2020). The oceanic forcing is based on a retreat parameterization for tidewater glaciers, forced by MAR run-off and ocean temperature changes in seven drainage basins around Greenland (Slater et al. 2019, 2020).

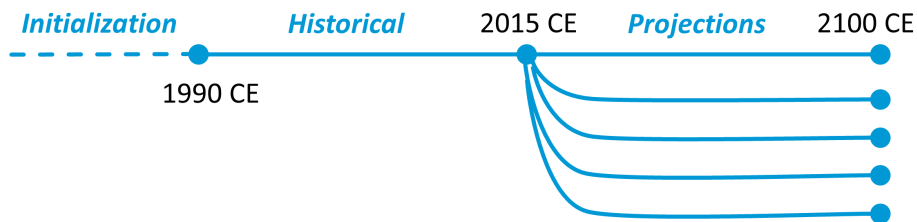


Figure 1: ISMIP6 experimental design. A model-specific initialization is followed by a historical simulation from 1990 until 2015. The several projections run from 2015 until the end of 2100. (Credit: Martin Rückamp, AWI Bremerhaven, Germany.)

Here, we describe the ISMIP6 future projections for the Greenland ice sheet carried out with the ice-sheet model SICOPOLIS (SIMulation COde for POLythermal Ice Sheets). The emphasis is on the model-specific features that are not covered in detail in the community papers (Goelzer et al. 2020, Payne et al. 2020). For the ISMIP6 future projections for the Antarctic ice sheet, see the companion document by Greve et al. (2020).

2 Ice-sheet model SICOPOLIS v5.1

The three-dimensional, dynamic/thermodynamic model SICOPOLIS was originally created in a version for the Greenland ice sheet (Greve 1995, 1997a,b). Since then, the model has been developed continuously and applied to problems of past, present and future glaciation of Greenland, Antarctica, the entire northern hemisphere, the polar ice caps of

the planet Mars and others, resulting in more than 120 publications in the peer-reviewed literature (www.sicopolis.net, last accessed 2020-08-28).

Here, we apply SICOPOLIS v5.1 (Greve and SICOPOLIS Developer Team 2019) to the Greenland ice sheet. The model domain covers the entire area of Greenland and the surrounding oceans. We use the EPSG:3413 grid, based on a polar stereographic projection with the WGS 84 reference ellipsoid, standard parallel 70°N and central meridian 45°W. The stereographic plane is spanned by the Cartesian coordinates x and y , and the coordinate z points upward. It is discretized by a regular (structured) grid with $\Delta x = 5$ or 10 km resolution. In the vertical, we use terrain-following coordinates (sigma transformation) with 81 layers in the ice domain and 41 layers in the thermal lithosphere layer below.

For the ice rheology, we use the regularized Glen flow law in the form of Greve and Blatter (2009, Sect. 4.3.2). The dynamics of grounded ice is modelled by either the shallow-ice approximation (SIA) or a hybrid SIA–SStA formulation (SStA: shelfy-stream approximation). The latter, abbreviated as ‘HYB’ in the following, is a modified form of Bernales et al.’s (2017) HS-1 scheme (hybrid scheme #1), which is described in detail in the companion document (Greve et al. 2020, Sect. 2). Floating ice is ignored. Ice thermodynamics is modelled by the one-layer melting-CTS enthalpy scheme (CTS: cold-temperate transition surface; Blatter and Greve 2015, Greve and Blatter 2016). The temperature-dependent rate factor for cold ice is by Cuffey and Paterson (2010, Sect. 3.4.6), and the water-content-dependent rate factor for temperate ice is by Lliboutry and Duval (1985).

The ice surface is assumed to be traction-free. Basal sliding under grounded ice, v_b , is described by a Weertman-Budd-type sliding law accounting for sub-melt sliding (Hindmarsh and Le Meur 2001) and the subglacial water-layer thickness (Kleiner and Humbert 2014, Calov et al. 2018):

$$v_b = -C_b \frac{\tau_b^p}{N_b^q}, \quad (1)$$

with

$$C_b = C_b^0 \exp\left(\frac{T_b'}{\gamma}\right) \left[1 + c\left(1 - \exp\left(-\frac{H_w}{H_w^0}\right)\right)\right]. \quad (2)$$

In Eq. (1), C_b is the sliding function, τ_b the basal drag (shear stress), N_b the basal normal stress (counted positive for compression; here assumed to be equal to the stress exerted by the overburden ice only, i.e., the counteracting water pressure is neglected), and p and q are the sliding exponents. In Eq. (2), C_b^0 is the sliding coefficient, T_b' the basal temperature relative to pressure melting (in °C, always $\leq 0^\circ\text{C}$), γ the sub-melt-sliding parameter, c the coefficient for water-layer-enhanced basal sliding, H_w the subglacial water-layer thickness and H_w^0 the threshold water-layer thickness. Optionally, the simulated ice sheet can be divided into $n = 1 \dots N$ regions, for which individual basal sliding coefficients $(C_b^0)_n$ are set. We do this for $N = 20$ regions, the 19 basins by Zwally et al. (2012) plus a separate region for the North-East Greenland Ice Stream (NEGIS), defined by a surface velocity $\geq 50 \text{ m a}^{-1}$ (Smith-Johnsen et al. 2020a,b); see Sects. 3.2.2 and 3.2.3. The water-layer thickness H_w is computed by a steady-state routing scheme for subglacial water that receives its input from the basal melting rate under grounded ice (Le Brocq et al. 2006, 2009).

The bed topography is BedMachine v3 (Morlighem et al. 2017). Glacial isostatic adjustment (GIA) is included using a local-lithosphere–relaxing–asthenosphere (LLRA) model

Quantity	Value
Density of ice, ρ	910 kg m ⁻³
Density of sea water, ρ_{sw}	1028 kg m ⁻³
Gravitational acceleration, g	9.81 m s ⁻²
Length of year, 1 a	31 556 926 s
Power-law exponent, n	3
Residual stress, σ_0	10 kPa
Flow enhancement factor, E	1 / 3*
Melting temperature at low pressure, T_0	273.16 K
Clausius-Clapeyron gradient, β	8.7×10^{-4} K m ⁻¹
Universal gas constant, R	8.314 J mol ⁻¹ K ⁻¹
Heat conductivity of ice, κ	$9.828 e^{-0.0057 T[\text{K}]}$ W m ⁻¹ K ⁻¹
Specific heat of ice, c	$(146.3 + 7.253 T[\text{K}])$ J kg ⁻¹ K ⁻¹
Latent heat of ice, L	3.35×10^5 J kg ⁻¹
Sliding exponents, (p, q)	(3, 2)
Sub-melt-sliding parameter, γ	1°C
Coefficient for water-layer-enhanced basal sliding, c	9
Threshold water-layer thickness, H_w^0	5 mm
Density \times specific heat of the lithosphere, $\rho_l c_l$	2000 kJ m ⁻³ K ⁻¹
Heat conductivity of the lithosphere, κ_l	3 W m ⁻¹ K ⁻¹
Thickness of the thermal upper boundary layer of the lithosphere, H_{lt}	2 km
Asthenosphere density, ρ_a	3300 kg m ⁻³
Time lag for the relaxing asthenosphere, τ_a	3000 a

Table 1: Physical parameters used for the simulations of this study.

*: $E = 1$ for Holocene or Eemian ice (deposited not earlier than 11 ka BP, or between 132 and 114 ka BP), $E = 3$ for Weichselian or pre-Eemian ice (deposited during other times).

(Le Meur and Huybrechts 1996). The geothermal heat flux is by Greve (2019), applied at the base of the thermal lithosphere layer (rather than directly at the ice base) to account for the thermal inertia of the lithosphere (Ritz 1987). The physical parameters are listed in Table 1.

3 Initialization via paleoclimatic spin-up

A crucial prerequisite for future projections is a reasonable initial state of the ice sheet regarding ice geometry, surface velocities and englacial temperature (Goelzer et al. 2018, Seroussi et al. 2019). Here, we produce this initial state by carrying out a paleoclimatic spin-up over a full glacial cycle (134 ka) until the year 1990 CE (which corresponds to the time $t = 0$). It is similar to the spin-ups described by Rückamp et al. (2019) and Greve (2019).

3.1 Climate forcing

The climatic forcing for the spin-up consists of time-dependent distributions of the surface temperature and precipitation. For the present-day mean annual and mean-July surface temperature, we employ the parameterizations by Fausto et al. (2009). These parameterizations express the temperature distributions as linear functions of surface elevation, latitude and longitude. However, the parameterizations are valid for 1996–2006, whereas our reference year (time $t = 0$) is 1990. In order to correct for this difference, we apply an offset of -1°C to both parameterizations. This value was estimated based on the data shown by Kobashi et al. (2011, Fig. 1 therein).

The main, time-dependent driver for the paleoclimatic spin-up is the surface temperature anomaly $\Delta T(t)$, assumed to be spatially uniform over the Greenland ice sheet. It is based on the $\delta^{18}\text{O}$ record from the NGRIP ice core (North Greenland Ice Core Project members 2004) on the GICC05modelext time scale (Wolff et al. 2010), converted to temperature with the $\Delta T/\delta^{18}\text{O}$ transfer factor of $2.4^\circ\text{C}\text{‰}^{-1}$ by Nielsen et al. (2018) (based on Huybrechts 2002). Warming during the Eemian is capped at $\Delta T = +4.5^\circ\text{C}$ (otherwise, the Eemian Greenland ice sheet becomes unrealistically small). The record is extended into the penultimate glacial by assuming $\Delta T = -20^\circ\text{C}$ at 140 ka b2k (before the year 2000) and a linear increase since then. For the most recent 4 ka, the surface temperature anomaly derived for the GISP2 site by Kobashi et al. (2011) is used instead of the NGRIP record. In addition, we prescribe the sea-level history, which is derived from the SPECMAP (Spectral Mapping Project) marine $\delta^{18}\text{O}$ record (Imbrie et al. 1984).

For the present-day precipitation, we use monthly means for the period 1958–2001, created with the regional energy and moisture balance model REMBO (Robinson et al. 2010). For any other time t , we assume a 7.3% change of the precipitation rate for every 1°C of surface temperature (ΔT) change (Huybrechts 2002). Conversion from precipitation to snowfall rate (solid precipitation) is done on a monthly-mean basis using the empirical fifth-order polynomial function by Bales et al. (2009). As in the study by Greve and Herzfeld (2013), surface melting is parameterized by Reeh’s (1991) positive degree day (PDD) method, supplemented by the semi-analytical solution for the PDD integral by Calov and Greve (2005). The PDD factors are $\beta_{\text{ice}} = 8\text{ mm WE d}^{-1}\text{ }^\circ\text{C}^{-1}$ and

$\beta_{\text{snow}} = 3 \text{ mm WE d}^{-1} \text{ } ^\circ\text{C}^{-1}$ for ice and snow melt, respectively (where WE means water equivalent) (Huybrechts and de Wolde 1999). Furthermore, the standard deviation of short-term, statistical air temperature fluctuations is $\sigma = 5^\circ\text{C}$, and the saturation factor for the formation of superimposed ice is chosen as $P_{\text{max}} = 0.6$ (Reeh 1991).

We start the spin-up at $t = -134 \text{ ka}$. At that time, $\Delta T = -11.13^\circ\text{C}$, which is close to the mean anomaly over the whole period (Rückamp et al. 2019, Greve 2019).

3.2 Spin-up sequence

3.2.1 10 km resolution, SIA dynamics, $t = -134 \dots -9 \text{ ka}$

(1) Simulation grl10_bm3_paleo17a

Time $t = -134 \dots -9 \text{ ka}$, starting from the observed present-day topography. The initial temperature field is computed by the Robin (1955) solution for grounded ice columns with positive SMB and a linear profile otherwise (SICOPOLIS parameter TEMP_INIT = 4). Time steps: $\Delta t = 1 \text{ a}$ (for dynamics and topography), $\Delta t_{\text{temp}} = 1 \text{ a}$ (for thermodynamics). SIA dynamics, free evolution of the ice topography. Basal sliding with a constant sliding parameter $C_b^0 = 2.5 \text{ m a}^{-1} \text{ Pa}^{-1}$ after -129 ka . During the first 5 ka (prior to -129 ka), basal sliding is ramped up according to Rückamp et al. (2019, Sect. 3.1, run (1)) (see also Greve et al. 2020, Sect. 3.2.1, run (2)).

3.2.2 5 km resolution, SIA dynamics, $t = -9 \dots 0 \text{ ka}$

(2) Simulation grl05_bm3_paleo17_init10a

Short simulation over 10 a, starting from the observed present-day topography, no basal sliding, isothermal conditions ($T = -10^\circ\text{C}$ everywhere). Time steps: $\Delta t = \Delta t_{\text{temp}} = 0.1 \text{ a}$. SIA dynamics, free evolution of the ice topography. The purpose of this run is to produce a slightly smoothed present-day topography (surface $h_{\text{target}}(x, y)$, bed $b_{\text{target}}(x, y)$) of the Greenland ice sheet that serves as a target for all subsequent runs that employ topography nudging.

(3) Simulation grl05_bm3_paleo17b

Time $t = -9 \dots 0 \text{ ka}$, starting from the resolution-doubled output of run (1) at $t = -9 \text{ ka}$. Time steps: $\Delta t = \Delta t_{\text{temp}} = 0.5 \text{ a}$. SIA dynamics. Basal sliding with a constant sliding parameter $C_b^0 = 2.5 \text{ m a}^{-1} \text{ Pa}^{-1}$. The computed topography is continuously nudged towards the output of run (2) by using the method by Rezvanbehbahani et al. (2019) and Rückamp et al. (2019) (see also Greve et al. (2020, Sect. 3.2.1, run (2)); SICOPOLIS parameter THK_EVOL = 3).

(4) Simulations grl05_bm3_paleo17b-{01,02,03,04,05,06,07}

Each of these seven runs reads the output of run (3) at $t = -1 \text{ ka}$ and runs until $t = 0$. Time steps: $\Delta t = \Delta t_{\text{temp}} = 0.5 \text{ a}$. The basal sliding coefficients $(C_b^0)_n^k$ ($n = 1 \dots 20$) are iteratively adjusted for the 20 regions described above (Sect. 2) to achieve optimum agreement between simulated and observed surface velocities in these regions. The index k counts the iterations. The starting value (iteration

no. $k = 0$) is the value from run (3), $(C_b^0)_n^0 = 2.5 \text{ m a}^{-1} \text{ Pa}^{-1}$. Except for the basal sliding, the set-up is the same as that of run (3).

The k -th iteration of the run is called `grl05_bm3_paleo17b- k` . For each basin n , we compute a regression line for simulated vs. observed surface velocities (within the range $[10 \text{ m a}^{-1}, 10000 \text{ m a}^{-1}]$) through the origin with the slope a_n^k , and update the sliding coefficient $(C_b^0)_n^k$. This is described in detail in the companion document (Greve et al. 2020, Sect. 3.2.3, Eqs. (16)–(21)).

The procedure is stopped after $k = 7$ iterations (`grl05_bm3_paleo17b-07`), when the overall slope (for the entire ice sheet) has reached the interval $[0.95, 1.05]$: $a_{\text{all}}^7 = 1.0472$. Figure 2 demonstrates that the scheme has converged well; further iterations would not lead to a significant improvement of the fit.

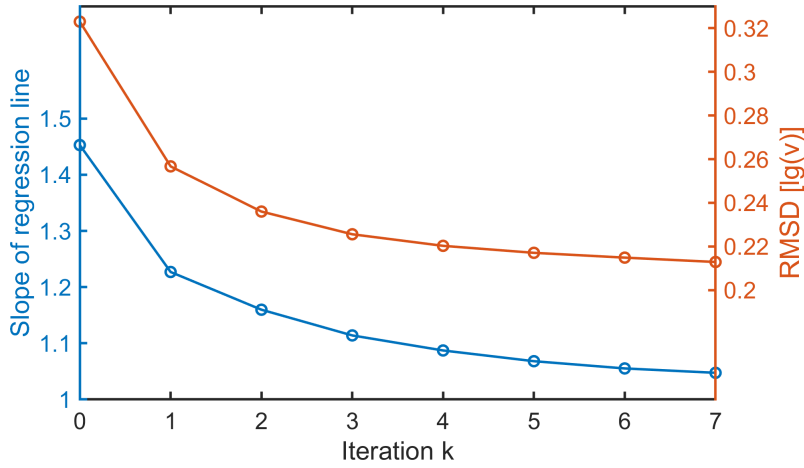


Figure 2: Slope a_{all}^k of the regression line for the entire ice sheet and RMSD (root mean square deviation) of the logarithmic surface velocity $\lg(v)$ (in m a^{-1}) for the entire ice sheet after k iterations.

(5a) Simulation `grl05_bm3_paleo22b-07`

Essentially a repetition of the final run (4) (`grl05_bm3_paleo17b-07`); however, with a modified set-up:

All runs (1)–(4) use an over-implicit scheme for solving the diffusive SIA ice-thickness equation ($\text{OVI}/w = 1.5$ in the terminology by Greve and Calov (2002); SICOPOLIS parameter $\text{CALCTHK} = 2$). While this scheme has favourable stability properties, thus allowing large dynamics time steps Δt , the way the diffusivity is treated (Type II in the terminology by Huybrechts et al. (1996), see their Eq. (19) and accompanying text) is not inherently mass-conserving. For the high resolution employed here and the correspondingly variable structure of the bed topography, this leads to a significant residual when trying to close the global mass balance for the ice sheet (change of volume with time equals total SMB, basal melting and discharge/calving). To avoid this, we switch to an explicit solver that discretizes the advection term of the general ice-thickness equation by a mass-conserving scheme in an upwind flux form (Calov et al. 2018, their Eq. (A1); SICOPOLIS parameter $\text{CALCTHK} = 4$).

This solver requires a greatly reduced dynamics time step of $\Delta t = 0.02$ a, while the thermodynamics time step $\Delta t_{\text{temp}} = 0.5$ a can be retained.

Topography nudging is changed from the method described above (see run (3)) to the implied SMB by Calov et al. (2018) (their Eq. (10) with a relaxation time $\tau_{\text{relax}} = 100$ a) (SICOPOLIS parameters THK_EVOL = 1, ACCSURFACE = 7, ABL-SURFACE = 7). Further, marine-ice formation is enabled (SICOPOLIS parameter MARGIN = 2) with a minimum sea-bed elevation of -300 m.

(6a) Simulations grl05_bm3_paleo22b-{08,09}

Two further iteration steps for the regional basal sliding coefficients with the modified set-up of run (5a), reading the output of run (5) at $t = -100$ a and running until $t = 0$. Time steps: $\Delta t = 0.02$ a, $\Delta t_{\text{temp}} = 0.5$ a.

The resulting basal sliding coefficients (Fig. 3) show a great variability. By far the largest value occurs in region No. 6, which is the NEGIS region, followed by Nos. 17 and 16, which are the Jakobshavn drainage basin and the adjacent basin to the south, respectively.

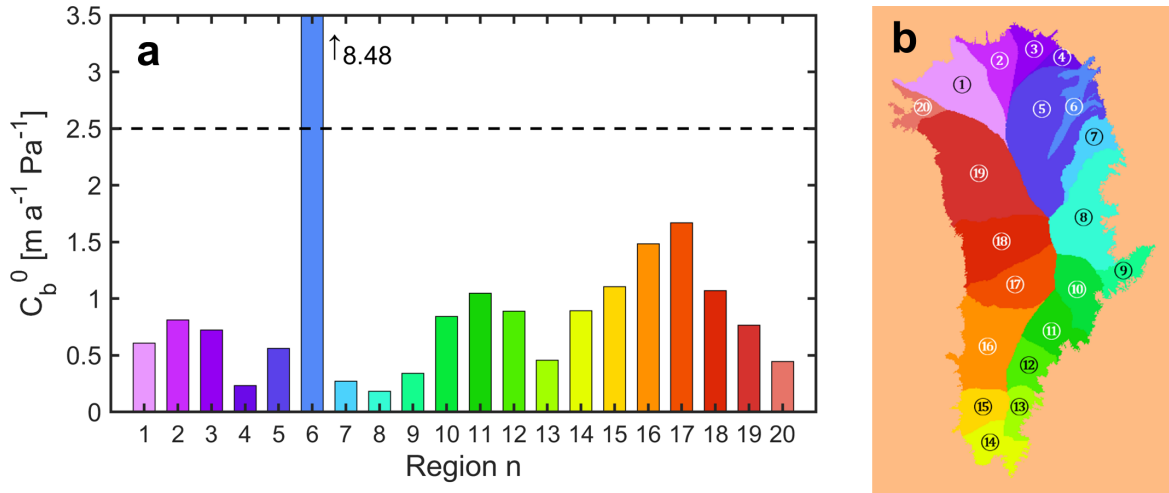


Figure 3: (a) Basal sliding coefficients $(C_b^0)_n$ for the 20 regions (19 basins by Zwally et al. (2012) plus a separate NEGIS region) obtained for SIA dynamics. (b) Location of the regions, marked by circled numbers that correspond to the region number n in panel (a).

(7a) Simulation grl05_bm3_paleo22c-09

Time $t = -1 \dots 0$ ka, starting from the output of run (3) at $t = -1$ ka. Otherwise, same set-up as the final run (6a).

(8a) Simulation grl05_bm3_paleo22d-09

Time $t = -120 \dots 0$ a, re-run of the last 120 a of run (7a) with annual output of scalar and 2D fields as requested by the ISMIP6 protocol. The final state of this run is our initial ice sheet for the year 1990 CE with SIA dynamics.

3.2.3 5 km resolution, HYB dynamics, $t = -1 \dots 0$ ka

(5b) Simulation grl05_bm3_paleo23b-07

Like run (5a), but with HYB dynamics (modified HS-1 scheme, see Sect. 2). Time $t = -1 \dots 0$ ka. Time steps $\Delta t = 0.02$ a, $\Delta t_{\text{temp}} = 0.5$ a.

(6b) Simulation grl05_bm3_paleo23c-{08,09}

Two further iteration steps for the regional basal sliding coefficients with the set-up of run (5b). Time $t = -1 \dots 0$ ka. Time steps $\Delta t = 0.02$ a, $\Delta t_{\text{temp}} = 0.5$ a.

Note that this differs from the SIA runs (6a), where the two iterations were carried out only for 100 a.

Figure 4 shows the resulting basal sliding coefficients. The distribution has not changed significantly compared to the SIA case (Fig. 3). However, the value for the NEGIS region (No. 6) has become even larger, and region No. 16 (south of Jakobs-havn) features now a slightly larger sliding coefficient than No. 17 (Jakobshavn).

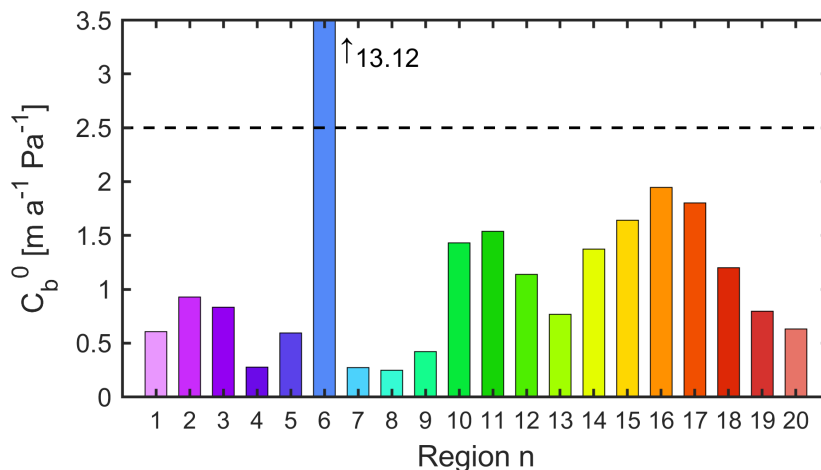


Figure 4: Basal sliding coefficients (C_b^0)_n for the 20 regions (19 basins by Zwally et al. (2012) plus a separate NEGIS region, see Fig. 3b) obtained for HYB dynamics.

(7b) Simulation grl05_bm3_paleo23d-09

Time $t = -120 \dots 0$ a, re-run of the last 120 a of the final run (6b) with annual output of scalar and 2D fields as requested by the ISMIP6 protocol. The final state of this run is our initial ice sheet for the year 1990 CE with HYB dynamics.

3.3 Simulated initial (1990 CE) ice sheet

For the HYB case, the spin-up sequence produces an initial ice sheet with a total volume of $V = 2.940 \times 10^6 \text{ km}^3$, a volume above flotation of $V_{\text{af}} = 7.279$ m SLE (sea-level equivalent) and an ice area of $A = 1.781 \times 10^6 \text{ km}^2$. For SIA, the values are very similar, $V = 2.934 \times 10^6 \text{ km}^3$, $V_{\text{af}} = 7.264$ m SLE and $A = 1.781 \times 10^6 \text{ km}^2$.

In the following, we will focus on the HYB case (more sophisticated ice dynamics) and report the SIA results only briefly for comparison. Due to the topography nudging

applied during the last 9 ka of the spin-up, the simulated ice thickness agrees well with its observed counterpart (Fig. 5). In the interior ice sheet, the misfit is typically of the order of 10 m only. Closer to the coast, larger misfits occur, mainly in areas of fast-flowing ice streams like 79 N Glacier, Zachariae Ice Stream (NEGIS outlets) and Petermann Glacier where the floating ice tongues are missing in the simulation. The RMSD (root mean square deviation) is 55.6 m (SIA: 59.3 m).

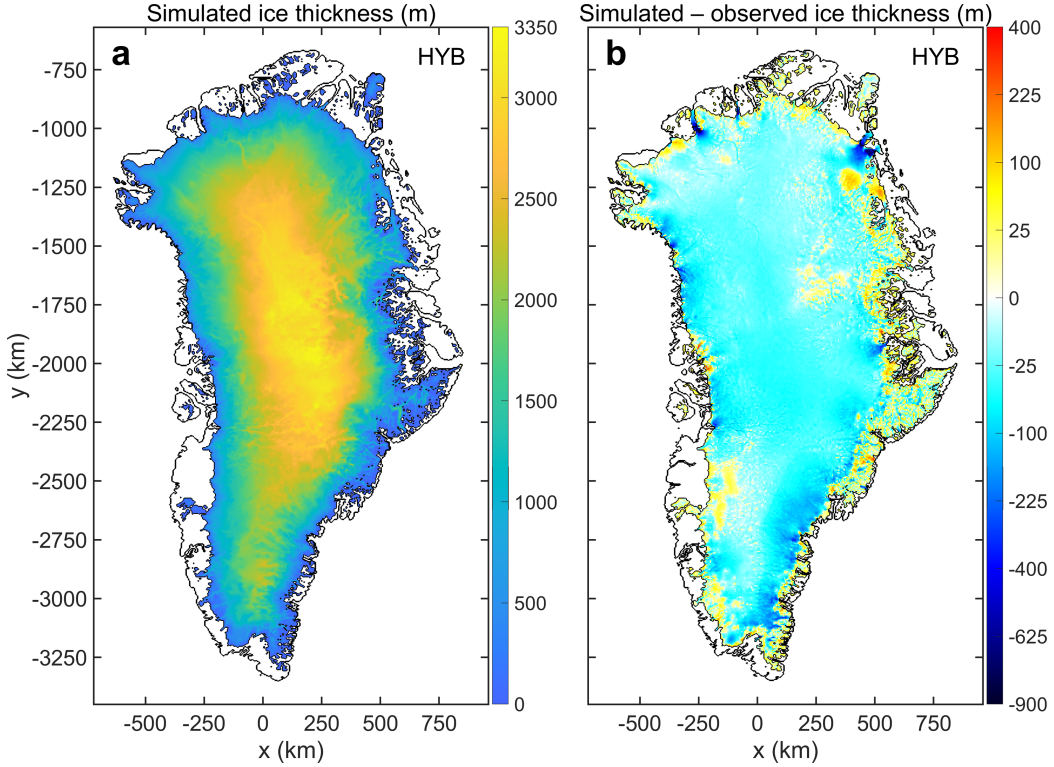


Figure 5: Spin-up simulation (HYB): (a) Simulated initial (1990 CE) ice thickness. (b) Simulated minus observed (Morlighem et al. 2017) ice thickness on a square-root scale.

The simulated surface-velocity field for the initial state of the Greenland ice sheet is shown in Fig. 6. Overall, it agrees well with the observations. The large-scale structure, as well as most of the smaller-scale features, in particular the major ice streams and outlet glaciers, are well reproduced. The RMSD is 101.7 m a^{-1} (SIA: 88.1 m a^{-1}). Grid points located at the simulated ice margin (with an ice-free neighbour point) have been excluded from this computation because they sometimes feature unrealistically high velocities due to the constraint that the simulated ice sheet cannot extend past the observed margin (which is a feature of the implied SMB).

From the last 30 years of both the HYB and SIA spin-ups, we extract 1960–1989 reference climatologies. For HYB, it is shown in Fig. 7. The SMB results from the implied SMB (Sect. 3.2). This yields rather dry conditions [$\mathcal{O}(100 \text{ mm a}^{-1})$] in the interior ice sheet, generally larger positive SMB values closer to the coast and ablation zones at low elevations near the ice margin. However, patches of negative SMB also occur further inland. The ST distribution results from the parameterization described in Sect. 3.1 and shows the expected pattern with low temperatures in the interior, an increase towards the coast and a pronounced north-south gradient. The climatology for SIA is very similar.

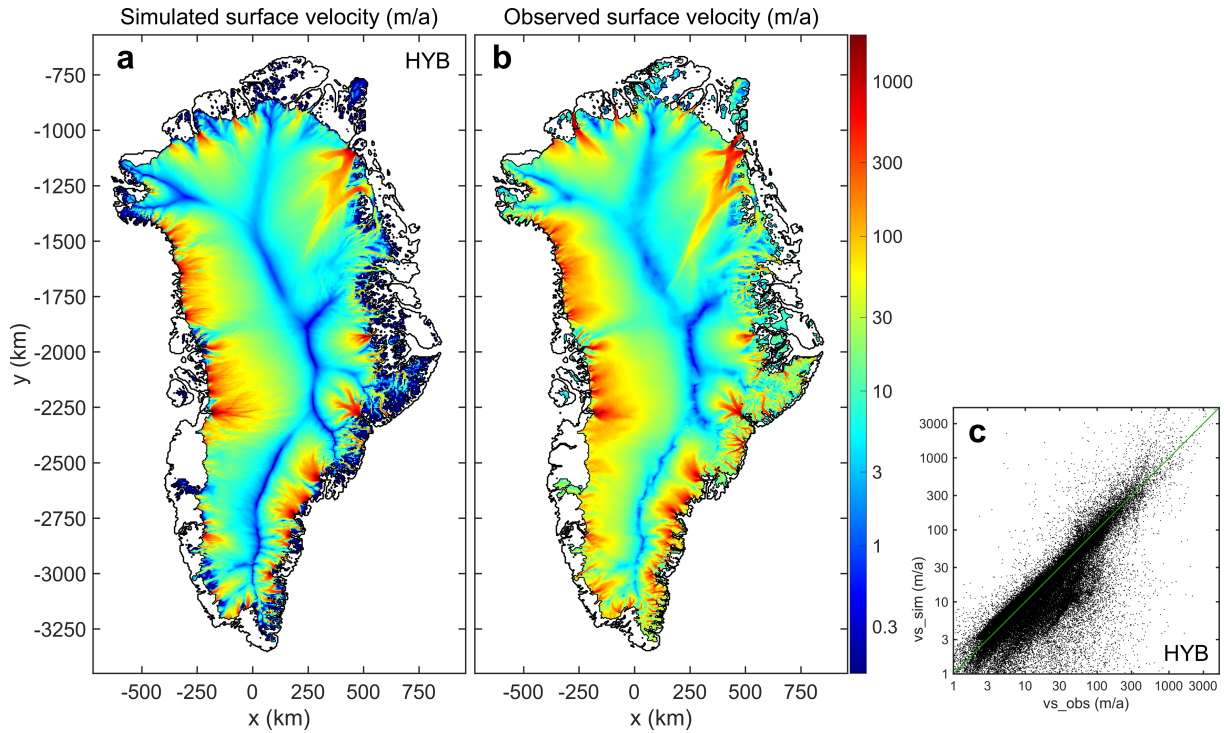


Figure 6: Spin-up simulation (HYB): (a) Simulated initial (1990 CE) vs. (b) observed (Joughin et al. 2016, 2018) surface-velocity fields. (c) Scatter plot of simulated vs. observed surface velocities. All velocities are shown on a logarithmic scale.

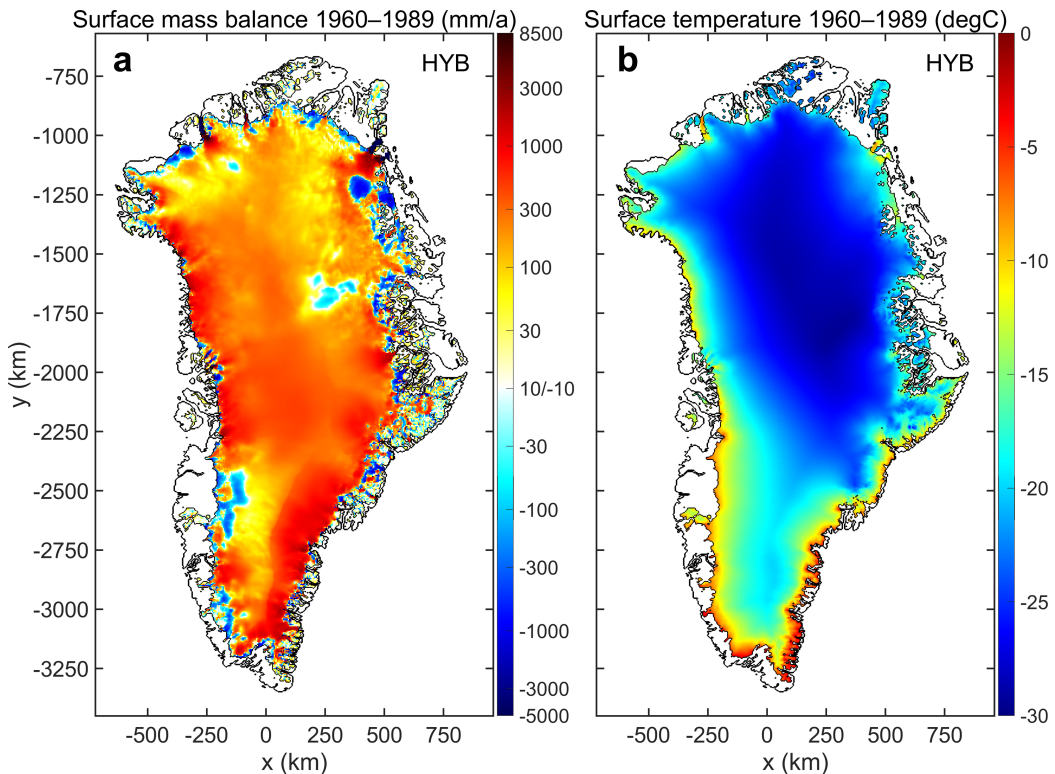


Figure 7: 1960–1989 reference climatology (HYB). (a) Surface mass balance (on a combined positive/negative logarithmic scale, in ice equivalents). (b) Surface temperature.

4 ISMIP6 future projections for Greenland

We now describe the experiments that run from the initialization date 1990 CE into the future. For all experiments, we use the regional basal sliding coefficients determined by the spin-up runs (6a) and (6b), respectively (Figs. 3a, 4). The time steps are the same as those of the spin-up runs (5a)–(8a) (SIA) and (5b)–(7b) (HYB): $\Delta t = 0.02$ a, $\Delta t_{\text{temp}} = 0.5$ a.

All experiments are carried out with SIA and HYB dynamics. Throughout this section, we will focus on HYB and refer to this case unless explicitly mentioned otherwise. The SIA results, which are very similar, will be reported only briefly for comparison.

4.1 Control runs, schematic experiment, historical run

We carry out a constant-climate control run (‘ctrl’) from 1990 until the end of 2100. It uses the ice sheet for 1990 that results from the spin-up as initial conditions. The time-independent forcing consists of our 1960–1989 reference climatology. Under these conditions, the ice sheet remains nearly stable, featuring only a very small mass gain of 0.76 mm SLE (SIA: 0.88 mm SLE) during the 111 years model time (not shown).

We repeat the initMIP-Greenland experiment ‘asmb’ (Goelzer et al. 2018) with the settings of this study. The set-up is that of ctrl, plus a time-dependent, schematic anomaly for the SMB. This produces a notable response of the ice sheet (Fig. 8, black dashed line): The increased melting around the ice margin leads to a mass loss of 127.0 mm SLE (SIA: 123.0 mm SLE). While the quantitative interpretability of this result is limited due to the schematic nature of the experiment, it illustrates well the sensitivity of the ice sheet to changing atmospheric forcing.

The historical run (‘hist’) bridges the gap between our initialization time 1990 and the start date of the projections in January 2015. Like ctrl and asmb, it starts from the 1990 ice sheet that results from the spin-up. Following the ISMIP6 recommendation (tinyurl.com/ismip6-wiki-gris, last accessed 2020-08-28), the climate forcing consists of the 1960–1989 reference climatology and the MIROC5 RCP8.5 SMB and ST anomalies. The ice sheet reacts only slightly, losing 3.3 mm SLE (SIA: 3.1 mm SLE) mass during the 25 years model time (Fig. 8, thick black solid line).

Following the ISMIP6 protocol, we conduct a second control run for January 2015 – December 2100, the same period that is used for the actual future climate experiments (see Sect. 4.2 below). This projection control run (‘ctrl_proj’) starts from the final state of the historical run and uses the 1960–1989 reference climatology as time-independent forcing. Similar to ctrl, the ice sheet remains nearly stable, showing only a slight mass gain of 1.7 mm SLE (SIA: 1.9 mm SLE) during the 86 years model time (Fig. 8, thin black solid line).

The SICOPOLIS names of the simulations described above are `grl05_bm3_future{22,23}-09_{ctrl,asmb,hist,ctrl_proj}` (‘22’ for SIA, ‘23’ for HYB).

4.2 Future climate experiments

The future climate experiments start from the final state of the historical run, and the model time is from January 2015 until December 2100. Their atmospheric forcing consists of the 1960–1989 reference climatology (see above), plus space-time-dependent anomalies

for the SMB, the ST and their vertical gradients. For the core (Tier 1) experiments, these anomalies were derived from three selected CMIP5 global climate models (GCMs) (Barthel et al. 2020). For the extended ensemble (Tier 2), three more CMIP5 GCMs were added, and a further extension (also Tier 2) includes four CMIP6 GCMs, the latter mainly chosen on the basis of early availability. The surface forcing generated by the CMIP GCMs was reinterpreted through the regional climate model MAR v3.9.6 (Delhasse et al. 2020). This also allowed to account for feedbacks due to height change by providing vertical SMB and ST gradients on each horizontal grid point (Franco et al. 2012). The ISMIP6 projections focus on the pessimistic “business as usual” scenarios RCP8.5 (CMIP5) or SSP5-8.5 (CMIP6). However, some experiments are also devised for the optimistic RCP2.6 (CMIP5) or SSP1-2.6 (CMIP6) scenarios that represent substantial emissions reductions. [RCP: Representative Concentration Pathway, SSP: Shared Socioeconomic Pathway.]

The oceanic forcing is the “retreat implementation” proposed by Slater et al. (2019, 2020). It relies on yearly average datasets of subglacial discharge per glacier and ocean thermal forcing (temperature minus freezing temperature) for 1950–2100 from the MAR-reprocessed CMIP GCM simulations. These datasets are used to create projections of marine-terminating glacier retreat for 2015–2100. Since ice-sheet models with a resolution similar to that of SICOPOLIS (5 km) may not capture small outlet glaciers well and may have distinct locations for individual outlet glaciers compared to the observations, average retreat rates are provided for seven ice–ocean sectors around Greenland.

#	exp_id	Scenario	GCM	Ocean forcing	
5	exp05	RCP8.5	MIROC5	Medium	Core experiments (Tier 1)
6	exp06	RCP8.5	NorESM1-M	Medium	
7	exp07	RCP2.6	MIROC5	Medium	
8	exp08	RCP8.5	HadGEM2-ES	Medium	
9	exp09	RCP8.5	MIROC5	High	
10	exp10	RCP8.5	MIROC5	Low	
A1	expa01	RCP8.5	IPSL-CM5A-MR	Medium	Extended ensemble (Tier 2)
A2	expa02	RCP8.5	CSIRO-Mk3.6.0	Medium	
A3	expa03	RCP8.5	ACCESS1.3	Medium	
B1	expb01	SSP5-8.5	CNRM-CM6-1	Medium	CMIP6 extension (Tier 2)
B2	expb02	SSP1-2.6	CNRM-CM6-1	Medium	
B3	expb03	SSP5-8.5	UKESM1-0-LL	Medium	
B4	expb04	SSP5-8.5	CESM2	Medium	
B5	expb05	SSP5-8.5	CNRM-ESM2-1	Medium	

Table 2: ISMIP6-Greenland Tier-1 and 2 future climate experiments discussed in this study. See Nowicki et al. (2020) for references for the GCMs. The SICOPOLIS names of these simulations are grl05_bm3_future{22,23}-09_<exp_id> (‘22’ for SIA, ‘23’ for HYB).

An overview of the ISMIP6 Tier-1 and Tier-2 experiments is given in Table 2. There are 14 experiments, 12 of which are for RCP8.5/SSP5-8.5 and two for RCP2.6/SSP1-2.6. In two experiments, the impact of different sensitivities of the retreat parameterization due to oceanic forcing (“high” and “low” vs. the normal, “medium” sensitivity) is tested.

[Further experiments employ an “open forcing”, in which the implementation of oceanic forcing is left to the discretion of the individual modellers. We have not conducted them with SICOPOLIS, so that they are not considered here.] For more details on the forcing, we refer to Nowicki et al. (2020) and Goelzer et al. (2020).

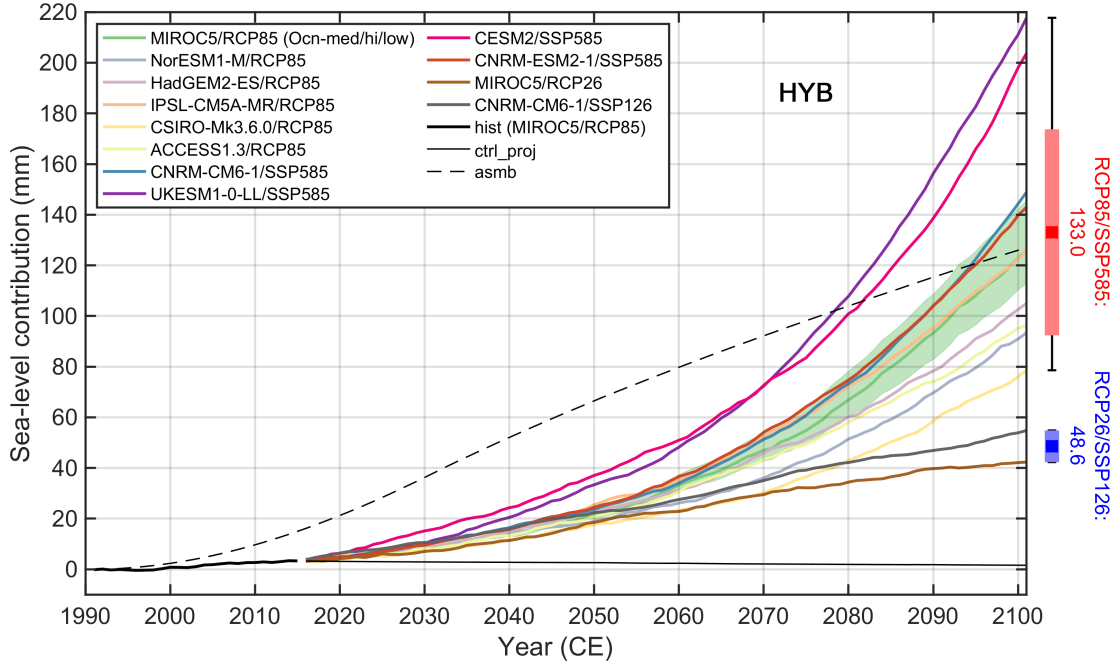


Figure 8: ISMIP6-Greenland historical run (hist), projection control run (ctrl_proj), schematic initMIP experiment (asmb) and Tier-1 and 2 future climate experiments for HYB dynamics: Simulated ice mass change, counted positively for loss and expressed as sea-level contribution. The red and blue boxes to the right show the mean ± 1 -sigma ranges for RCP8.5/SSP5-8.5 and RCP2.6/SSP1-2.6, respectively; the whiskers show the corresponding full ranges.

The contribution to sea-level change produced by these experiments is shown in Fig. 8 (coloured lines). Over the entire period from 1990 until 2100, it is 133.0 ± 40.7 mm (mean ± 1 -sigma uncertainty) for the RCP8.5/SSP5-8.5 experiments and 48.6 ± 6.2 mm for the RCP2.6/SSP1-2.6 experiments (SIA: 132.4 ± 40.4 mm for RCP8.5/SSP5-8.5, 48.0 ± 6.0 mm for RCP2.6/SSP1-2.6). The large difference between the results for the two pathways highlights the importance of efficient climate change mitigation for limiting the decay of the ice sheet.

The influence of the parameterization for ice retreat due to oceanic forcing is explored by Exps. #5, 9, 10 (MIROC5/RCP8.5 with “medium”, “high” and “low” sensitivity, respectively). The results are shown by the green line and green-shaded region in Fig. 8. By 2100, the simulated mass loss is $125.8^{+19.7}_{-13.0}$ mm SLE (SIA: $124.6^{+20.7}_{-12.9}$ mm SLE). Thus, the uncertainty due to these three calibrations is notable, but smaller than the uncertainty due to the GCM forcings.

For both RCP8.5/SSP5-8.5 and RCP2.6/SSP1-2.6 pathways, the CMIP6 GCMs produce a larger response of the ice sheet than the CMIP5 ones. While the significance of this statement is limited in case of RCP2.6/SSP1-2.6 (only one experiment each), the

picture is clearer for RCP8.5/SSP5-8.5, where the ensemble contains eight and four experiments forced by CMIP5 and CMIP6 GCMs, respectively. For the sake of comparability, we disregard Exps. #9 and 10 (varied sensitivity to oceanic forcing, see above), which leaves six experiments forced by CMIP5 GCMs. By 2100, the range of results is then 78.6–125.8 mm SLE for CMIP5 forcing vs. 143.0–217.7 mm SLE for CMIP6 forcing (SIA: 79.0–124.7 mm SLE for CMIP5 forcing, 142.5–217.0 mm SLE for CMIP6 forcing). Therefore, the projected sea-level contribution of the ice sheet under the newer CMIP6 SSP5-8.5 scenarios is significantly increased compared to the older CMIP5 RCP8.5 scenarios.

For a more detailed analysis of the future climate experiments, including results from other ice-sheet models, regional patterns etc., we refer to the ISMIP6 community papers by Goelzer et al. (2020) and Payne et al. (2020).

5 Summary

We described the ISMIP6 future projections for the Greenland ice sheet with the model SICOPOLIS, with a focus on the model-specific methods and set-up. Our paleoclimatic spin-up over 134 ka with successively refining resolution employed a topography nudging technique and an optimization of the basal sliding coefficients for 20 different regions to ensure a good match between the observed and the simulated initial (1990 CE) ice sheet. A historical run, forced by MIROC5/RCP8.5, brought the modelled ice sheet from this initial state to the projection start date January 2015. Our ensemble of 14 ISMIP6 Tier-1 and Tier-2 future climate experiments, forced by ten different CMIP5 and CMIP6 GCMs for two different pathways (RCP8.5/SSP5-8.5, RCP2.6/SSP1-2.6), forked off from there and was run until the end of the 21st century (December 2100).

The response of the ice sheet is mainly governed by a negative SMB due to increased surface melting in the near-margin (low-elevation) regions. Marine-terminating glacier retreat triggered by increasing ocean temperatures constitutes a further negative contribution to the total mass balance. Under RCP8.5/SSP5-8.5, this leads to a substantial projected mass loss during the 21st century, while the loss is much smaller under RCP2.6/SSP1-2.6. Efficient climate change mitigation is therefore crucial for limiting the contribution of the Greenland ice sheet to future sea-level rise. Results obtained with forcings from the newer CMIP6 GCMs consistently produced larger mass losses than those obtained with the older CMIP5 GCMs. By contrast, the choice of the ice-dynamics scheme, HYB vs. SIA, has only a minor effect on the results.

Additional ISMIP6 Tier-3 experiments have already been defined (ISMIP6 Steering Committee, personal communication 2019). They include experiments with atmosphere-only and ocean-only forcing and more sensitivity tests for the oceanic forcing. Further, we are planning to carry out simulations extending beyond 2100 to assess the longer-term response of the Greenland ice sheet to climate-change conditions.

Acknowledgements

We thank the Climate and Cryosphere (CliC) effort, which provided support for ISMIP6 through sponsoring of workshops, hosting the ISMIP6 website and wiki, and promoting ISMIP6. We acknowledge the World Climate Research Programme, which, through its Working Group on Coupled Modelling, coordinated and promoted CMIP5 and CMIP6. We thank the climate modelling groups for producing their model output and making it available; the Earth System Grid Federation (ESGF) for archiving the CMIP data and providing access to it; the University at Buffalo for ISMIP6 data distribution and upload; and the multiple funding agencies who support CMIP5, CMIP6, and ESGF. We thank the ISMIP6 steering committee, the ISMIP6 model selection group and ISMIP6 dataset preparation group for their continuous engagement in defining ISMIP6. This is ISMIP6 contribution No. 22.

Ralf Greve and Chris Chambers were supported by Japan Society for the Promotion of Science (JSPS) KAKENHI grant No. JP16H02224. Ralf Greve was supported by JSPS KAKENHI grant No. JP17H06104, by a Leadership Research Grant of Hokkaido University's Institute of Low Temperature Science (ILTS), and by the Arctic Challenge for Sustainability (ArCS) project of the Japanese Ministry of Education, Culture, Sports, Science and Technology (MEXT) (program grant number JPMXD1300000000). Reinhard Calov was funded by the PalMod project (PalMod 1.1 and 1.3 with grants 01LP1502C and 01LP1504D) of the German Federal Ministry of Education and Research (BMBF).

References

- Bales, R. C., Guo, Q., Shen, D., McConnell, J. R., Du, G., Burkhart, J. F., Spikes, V. B., Hanna, E., and Cappelen, J.: Annual accumulation for Greenland updated using ice core data developed during 2000–2006 and analysis of daily coastal meteorological data, *Journal of Geophysical Research: Atmospheres*, 114, D06 116, <https://doi.org/10.1029/2008JD011208>, 2009.
- Barthel, A., Agosta, C., Little, C. M., Hattermann, T., Jourdain, N. C., Goelzer, H., Nowicki, S., Seroussi, H., Straneo, F., and Bracegirdle, T. J.: CMIP5 model selection for ISMIP6 ice sheet model forcing: Greenland and Antarctica, *The Cryosphere*, 14, 855–879, <https://doi.org/10.5194/tc-14-855-2020>, 2020.
- Bernales, J., Rogozhina, I., Greve, R., and Thomas, M.: Comparison of hybrid schemes for the combination of shallow approximations in numerical simulations of the Antarctic Ice Sheet, *The Cryosphere*, 11, 247–265, <https://doi.org/10.5194/tc-11-247-2017>, 2017.
- Blatter, H. and Greve, R.: Comparison and verification of enthalpy schemes for polythermal glaciers and ice sheets with a one-dimensional model, *Polar Science*, 9, 196–207, <https://doi.org/10.1016/j.polar.2015.04.001>, 2015.
- Calov, R. and Greve, R.: A semi-analytical solution for the positive degree-day model with stochastic temperature variations, *Journal of Glaciology*, 51, 173–175, <https://doi.org/10.3189/172756505781829601>, 2005.
- Calov, R., Beyer, S., Greve, R., Beckmann, J., Willeit, M., Kleiner, T., Rückamp, M., Humbert, A., and Ganopolski, A.: Simulation of the future sea level contribution of Greenland with a new glacial system model, *The Cryosphere*, 12, 3097–3121, <https://doi.org/10.5194/tc-12-3097-2018>, 2018.

- Cuffey, K. M. and Paterson, W. S. B.: *The Physics of Glaciers*, Elsevier, Amsterdam, The Netherlands etc., 4th edn., 2010.
- Delhasse, A., Kittel, C., Amory, C., Hofer, S., van As, D., S. Fausto, R., and Fettweis, X.: Brief communication: Evaluation of the near-surface climate in ERA5 over the Greenland Ice Sheet, *The Cryosphere*, 14, 957–965, <https://doi.org/10.5194/tc-14-957-2020>, 2020.
- Eyring, V., Bony, S., Meehl, G. A., Senior, C. A., Stevens, B., Stouffer, R. J., and Taylor, K. E.: Overview of the Coupled Model Intercomparison Project Phase 6 (CMIP6) experimental design and organization, *Geoscientific Model Development*, 9, 1937–1958, <https://doi.org/10.5194/gmd-9-1937-2016>, 2016.
- Fausto, R. S., Ahlstrøm, A. P., van As, D., Bøggild, C. E., and Johnsen, S. J.: A new present-day temperature parameterization for Greenland, *Journal of Glaciology*, 55, 95–105, <https://doi.org/10.3189/002214309788608985>, 2009.
- Fettweis, X., Box, J. E., Agosta, C., Amory, C., Kittel, C., Lang, C., van As, D., Machguth, H., and Gallée, H.: Reconstructions of the 1900–2015 Greenland ice sheet surface mass balance using the regional climate MAR model, *The Cryosphere*, 11, 1015–1033, <https://doi.org/10.5194/tc-11-1015-2017>, 2017.
- Franco, B., Fettweis, X., Lang, C., and Erpicum, M.: Impact of spatial resolution on the modelling of the Greenland ice sheet surface mass balance between 1990–2010, using the regional climate model MAR, *The Cryosphere*, 6, 695–711, <https://doi.org/10.5194/tc-6-695-2012>, 2012.
- Goelzer, H., Nowicki, S., Edwards, T., Beckley, M., Abe-Ouchi, A., Aschwanden, A., Calov, R., Gagliardini, O., Gillet-Chaulet, F., Golledge, N. R., Gregory, J., Greve, R., Humbert, A., Huybrechts, P., Kennedy, J. H., Larour, E., Lipscomb, W. H., Le clec’h, S., Lee, V., Morlighem, M., Pattyn, F., Payne, A. J., Rodehacke, C., Rückamp, M., Saito, F., Schlegel, N., Seroussi, H., Shepherd, A., Sun, S., van de Wal, R., and Ziemen, F. A.: Design and results of the ice sheet model initialisation experiments initMIP-Greenland: an ISMIP6 intercomparison, *The Cryosphere*, 12, 1433–1460, <https://doi.org/10.5194/tc-12-1433-2018>, 2018.
- Goelzer, H., Nowicki, S., Payne, A., Larour, E., Seroussi, H., Lipscomb, W. H., Gregory, J., Abe-Ouchi, A., Shepherd, A., Simon, E., Agosta, C., Alexander, P., Aschwanden, A., Barthel, A., Calov, R., Chambers, C., Choi, Y., Cuzzone, J., Dumas, C., Edwards, T., Felikson, D., Fettweis, X., Golledge, N. R., Greve, R., Humbert, A., Huybrechts, P., Le clec’h, S., Lee, V., Leguy, G., Little, C., Lowry, D. P., Morlighem, M., Nias, I., Quiquet, A., Rückamp, M., Schlegel, N.-J., Slater, D., Smith, R., Straneo, F., Tarasov, L., van de Wal, R., and van den Broeke, M.: The future sea-level contribution of the Greenland ice sheet: a multi-model ensemble study of ISMIP6, *The Cryosphere*, 14, 3071–3096, <https://doi.org/10.5194/tc-14-3071-2020>, 2020.
- Greve, R.: *Thermomechanisches Verhalten polythermer Eisschilde – Theorie, Analytik, Numerik*, Doctoral thesis, Department of Mechanics, Darmstadt University of Technology, Germany, <https://doi.org/10.5281/zenodo.3815324>, 1995.
- Greve, R.: A continuum-mechanical formulation for shallow polythermal ice sheets, *Philosophical Transactions of the Royal Society A*, 355, 921–974, <https://doi.org/10.1098/rsta.1997.0050>, 1997a.

- Greve, R.: Application of a polythermal three-dimensional ice sheet model to the Greenland ice sheet: Response to steady-state and transient climate scenarios, *Journal of Climate*, 10, 901–918, [https://doi.org/10.1175/1520-0442\(1997\)010<0901:AOAPTD>2.0.CO;2](https://doi.org/10.1175/1520-0442(1997)010<0901:AOAPTD>2.0.CO;2), 1997b.
- Greve, R.: Geothermal heat flux distribution for the Greenland ice sheet, derived by combining a global representation and information from deep ice cores, *Polar Data Journal*, 3, 22–36, <https://doi.org/10.20575/00000006>, 2019.
- Greve, R. and Blatter, H.: *Dynamics of Ice Sheets and Glaciers*, Springer, Berlin, Germany etc., <https://doi.org/10.1007/978-3-642-03415-2>, 2009.
- Greve, R. and Blatter, H.: Comparison of thermodynamics solvers in the polythermal ice sheet model SICOPOLIS, *Polar Science*, 10, 11–23, <https://doi.org/10.1016/j.polar.2015.12.004>, 2016.
- Greve, R. and Calov, R.: Comparison of numerical schemes for the solution of the ice-thickness equation in a dynamic/thermodynamic ice-sheet model, *Journal of Computational Physics*, 179, 649–664, <https://doi.org/10.1006/jcph.2002.7081>, 2002.
- Greve, R. and Herzfeld, U. C.: Resolution of ice streams and outlet glaciers in large-scale simulations of the Greenland ice sheet, *Annals of Glaciology*, 54, 209–220, <https://doi.org/10.3189/2013AoG63A085>, 2013.
- Greve, R. and SICOPOLIS Developer Team: SICOPOLIS v5.1, Zenodo, <https://doi.org/10.5281/zenodo.3727511>, 2019.
- Greve, R., Calov, R., Obase, T., Saito, F., Tsutaki, S., and Abe-Ouchi, A.: ISMIP6 future projections for the Antarctic ice sheet with the model SICOPOLIS, Technical report, Zenodo, <https://doi.org/10.5281/zenodo.3971232>, 2020.
- Hindmarsh, R. C. A. and Le Meur, E.: Dynamical processes involved in the retreat of marine ice sheets, *Journal of Glaciology*, 47, 271–282, <https://doi.org/10.3189/172756501781832269>, 2001.
- Huybrechts, P.: Sea-level changes at the LGM from ice-dynamic reconstructions of the Greenland and Antarctic ice sheets during the glacial cycles, *Quaternary Science Reviews*, 21, 203–231, [https://doi.org/10.1016/S0277-3791\(01\)00082-8](https://doi.org/10.1016/S0277-3791(01)00082-8), 2002.
- Huybrechts, P. and de Wolde, J.: The dynamic response of the Antarctic and Greenland ice sheets to multiple-century climatic warming, *Journal of Climate*, 12, 2169–2188, [https://doi.org/10.1175/1520-0442\(1999\)012](https://doi.org/10.1175/1520-0442(1999)012), 1999.
- Huybrechts, P., Payne, A. J., and EISMINT Intercomparison Group: The EISMINT benchmarks for testing ice-sheet models, *Annals of Glaciology*, 23, 1–12, <https://doi.org/10.3189/S0260305500013197>, 1996.
- Imbrie, J., Hays, J. D., Martinson, D. G., McIntyre, A., Mix, A. C., Morley, J. J., Pisias, N. G., Prell, W. L., and Shackleton, N. J.: The orbital theory of Pleistocene climate: Support from a revised chronology of the marine $\delta^{18}\text{O}$ record, in: *Milankovitch and Climate, Part I*, edited by Berger, A., Imbrie, J., Hays, J., Kukla, G., and Saltzman, B., pp. 269–305, Reidel, Dordrecht, The Netherlands, NATO ASI Series C: Mathematical and Physical Sciences 126, 1984.

- Joughin, I., Smith, B. E., Howat, I. M., and Scambos, T.: MEaSURES multi-year Greenland ice sheet velocity mosaic, version 1, Dataset, NASA National Snow and Ice Data Center Distributed Active Archive Center, Boulder, Colorado, USA, <https://doi.org/10.5067/QUA5Q9SVMSJG>, 2016.
- Joughin, I., Smith, B. E., and Howat, I. M.: A complete map of Greenland ice velocity derived from satellite data collected over 20 years, *Journal of Glaciology*, 64, 1–11, <https://doi.org/10.1017/jog.2017.73>, 2018.
- Kleiner, T. and Humbert, A.: Numerical simulations of major ice streams in western Dronning Maud Land, Antarctica, under wet and dry basal conditions, *Journal of Glaciology*, 60, 215–232, <https://doi.org/10.3189/2014JoG13J006>, 2014.
- Kobashi, T., Kawamura, K., Severinghaus, J. P., Barnola, J.-M., Nakaegawa, T., Vinther, B. M., Johnsen, S. J., and Box, J. E.: High variability of Greenland surface temperature over the past 4000 years estimated from trapped air in an ice core, *Geophysical Research Letters*, 38, L21 501, <https://doi.org/10.1029/2011GL049444>, 2011.
- Le Brocq, A. M., Payne, A. J., and Siegert, M. J.: West Antarctic balance calculations: impact of flux-routing algorithm, smoothing algorithm and topography, *Computers & Geosciences*, 32, 1780–1795, <https://doi.org/10.1016/j.cageo.2006.05.003>, 2006.
- Le Brocq, A. M., Payne, A. J., Siegert, M. J., and Alley, R. B.: A subglacial water-flow model for West Antarctica, *Journal of Glaciology*, 55, 879–888, <https://doi.org/10.3189/002214309790152564>, 2009.
- Le Meur, E. and Huybrechts, P.: A comparison of different ways of dealing with isostasy: examples from modelling the Antarctic ice sheet during the last glacial cycle, *Annals of Glaciology*, 23, 309–317, <https://doi.org/10.3189/S0260305500013586>, 1996.
- Lliboutry, L. and Duval, P.: Various isotropic and anisotropic ices found in glaciers and polar ice caps and their corresponding rheologies, *Annales Geophysicae*, 3, 207–224, 1985.
- Morlighem, M., Williams, C. N., Rignot, E., An, L., Arndt, J. E., Bamber, J. L., Catania, G., Chauché, N., Dowdeswell, J. A., Dorschel, B., Fenty, I., Hogan, K., Howat, I., Hubbard, A., Jakobsson, M., Jordan, T. M., Kjeldsen, K. K., Millan, R., Mayer, L., Mouginot, J., Noël, B. P. Y., O’Cofaigh, C., Palmer, S., Rysgaard, S., Seroussi, H., Siegert, M. J., Slabon, P., Straneo, F., van den Broeke, M. R., Weinrebe, W., Wood, M., and Zinglensen, K. B.: BedMachine v3: Complete bed topography and ocean bathymetry mapping of Greenland from multibeam echo sounding combined with mass conservation, *Geophysical Research Letters*, 44, 11 051–11 061, <https://doi.org/10.1002/2017GL074954>, 2017.
- Nielsen, L. T., Aðalgeirsdóttir, G., Gkinis, V., Nuterman, R., and Hvidberg, C. S.: The effect of a Holocene climatic optimum on the evolution of the Greenland ice sheet during the last 10 kyr, *Journal of Glaciology*, 64, 477–488, <https://doi.org/10.1017/jog.2018.40>, 2018.
- North Greenland Ice Core Project members: High-resolution record of Northern Hemisphere climate extending into the last interglacial period, *Nature*, 431, 147–151, <https://doi.org/10.1038/nature02805>, 2004.

- Nowicki, S., Goelzer, H., Seroussi, H., Payne, A. J., Lipscomb, W. H., Abe-Ouchi, A., Agosta, C., Alexander, P., Asay-Davis, X. S., Barthel, A., Bracegirdle, T. J., Cullather, R., Felikson, D., Fettweis, X., Gregory, J. M., Hattermann, T., Jourdain, N. C., Kuipers Munneke, P., Larour, E., Little, C. M., Morlighem, M., Nias, I., Shepherd, A., Simon, E., Slater, D., Smith, R. S., Straneo, F., Trusel, L. D., van den Broeke, M. R., and van de Wal, R.: Experimental protocol for sea level projections from ISMIP6 stand-alone ice sheet models, *The Cryosphere*, 14, 2331–2368, <https://doi.org/10.5194/tc-14-2331-2020>, 2020.
- Nowicki, S. M. J., Payne, A., Larour, E., Seroussi, H., Goelzer, H., Lipscomb, W., Gregory, J., Abe-Ouchi, A., and Shepherd, A.: Ice Sheet Model Intercomparison Project (ISMIP6) contribution to CMIP6, *Geoscientific Model Development*, 9, 4521–4545, <https://doi.org/10.5194/gmd-9-4521-2016>, 2016.
- Payne, A. J., Nowicki, S., Abe-Ouchi, A., Agosta, C., Alexander, P., Albrecht, T., Asay-Davis, X., Barthel, A., Calov, R., Chambers, C., Choi, Y., Cullather, R., Cuzzone, J., Dumas, C., Edwards, T., Felikson, D., Fettweis, X., Goelzer, H., Gladstone, R., Golledge, N. R., Gregory, J. M., Greve, R., Hatterman, T., Hoffman, M. J., Humbert, A., Huybrechts, P., Jourdain, N. C., Kleiner, T., Larour, E., Le clec’h, S., Lee, V., Leguy, G., Lipscomb, W. H., Little, C. M., Lowry, D. P., Morlighem, M., Nias, I., Pattyn, F., Pelle, T., Price, S., Quiquet, A., Reese, R., Rückamp, M., Schlegel, N.-J., Seroussi, H., Shepherd, A., Simon, E., Slater, D., Smith, R., Straneo, F., Sun, S., Tarasov, L., Trusel, L. D., Van Breedam, J., van de Wal, R., van den Broeke, M., Winkelmann, R., Zhao, C., Zhang, T., and Zwinger, T.: Contrasting contributions to future sea level under CMIP5 and CMIP6 scenarios from the Greenland and Antarctic ice sheets, *Geophysical Research Letters*, submitted, 2020.
- Reeh, N.: Parameterization of melt rate and surface temperature on the Greenland ice sheet, *Polarforschung*, 59, 113–128, 1991.
- Rezvanbehbahani, S., Stearns, L. A., van der Veen, C. J., Oswald, G. K. A., and Greve, R.: Constraining the geothermal heat flux in Greenland at regions of radar-detected basal water, *Journal of Glaciology*, 65, 1023–1034, <https://doi.org/10.1017/jog.2019.79>, 2019.
- Ritz, C.: Time dependent boundary conditions for calculation of temperature fields in ice sheets, in: *The Physical Basis of Ice Sheet Modelling*, edited by Waddington, E. D. and Walder, J. S., IAHS Publication No. 170, pp. 207–216, IAHS Press, Wallingford, UK, 1987.
- Robin, G. de Q.: Ice movement and temperature distribution in glaciers and ice sheets, *Journal of Glaciology*, 2, 523–532, <https://doi.org/10.3198/1955JoG2-18-523-532>, 1955.
- Robinson, A., Calov, R., and Ganopolski, A.: An efficient regional energy-moisture balance model for simulation of the Greenland Ice Sheet response to climate change, *The Cryosphere*, 4, 129–144, <https://doi.org/10.5194/tc-4-129-2010>, 2010.
- Rückamp, M., Greve, R., and Humbert, A.: Comparative simulations of the evolution of the Greenland ice sheet under simplified Paris Agreement scenarios with the models SICOPOLIS and ISSM, *Polar Science*, 21, 14–25, <https://doi.org/10.1016/j.polar.2018.12.003>, 2019.
- Seroussi, H., Nowicki, S., Simon, E., Abe-Ouchi, A., Albrecht, T., Brondex, J., Cornford, S., Dumas, C., Gillet-Chaulet, F., Goelzer, H., Golledge, N. R., Gregory, J. M., Greve, R., Hoffman, M. J., Humbert, A., Huybrechts, P., Kleiner, T., Larour, E., Leguy, G., Lipscomb, W. H., Lowry, D., Mengel, M., Morlighem, M., Pattyn, F., Payne, A. J., Pollard, D., Price, S. F.,

- Quiquet, A., Reerink, T. J., Reese, R., Rodehacke, C. B., Schlegel, N.-J., Shepherd, A., Sun, S., Sutter, J., Van Breedam, J., van de Wal, R. S. W., Winkelmann, R., and Zhang, T.: InitMIP-Antarctica: an ice sheet model initialization experiment of ISMIP6, *The Cryosphere*, 13, 1441–1471, <https://doi.org/10.5194/tc-13-1441-2019>, 2019.
- Slater, D. A., Straneo, F., Felikson, D., Little, C. M., Goelzer, H., Fettweis, X., and Holte, J.: Estimating Greenland tidewater glacier retreat driven by submarine melting, *The Cryosphere*, 13, 2489–2509, <https://doi.org/10.5194/tc-13-2489-2019>, 2019.
- Slater, D. A., Felikson, D., Straneo, F., Goelzer, H., Little, C. M., Morlighem, M., Fettweis, X., and Nowicki, S.: Twenty-first century ocean forcing of the Greenland ice sheet for modelling of sea level contribution, *The Cryosphere*, 14, 985–1008, <https://doi.org/10.5194/tc-14-985-2020>, 2020.
- Smith-Johnsen, S., de Fleurian, B., Schlegel, N., Seroussi, H., and Nisancioglu, K.: Exceptionally high heat flux needed to sustain the Northeast Greenland Ice Stream, *The Cryosphere*, 14, 841–854, <https://doi.org/10.5194/tc-14-841-2020>, 2020a.
- Smith-Johnsen, S., Schlegel, N.-J., de Fleurian, B., and Nisancioglu, K. H.: Sensitivity of the Northeast Greenland Ice Stream to geothermal heat, *Journal of Geophysical Research: Earth Surface*, 125, e2019JF005252, <https://doi.org/10.1029/2019JF005252>, 2020b.
- Wolff, E. W., Chappellaz, J., Blunier, T., Rasmussen, S. O., and Svensson, A.: Millennial-scale variability during the last glacial: The ice core record, *Quaternary Science Reviews*, 29, 2828–2838, <https://doi.org/10.1016/j.quascirev.2009.10.013>, 2010.
- Zwally, H. J., Giovinetto, M. B., Beckley, M. A., and Saba, J. L.: Antarctic and Greenland drainage systems, GSFC Cryospheric Sciences Laboratory, Greenbelt, MD, USA, URL http://icesat4.gsfc.nasa.gov/cryo_data/ant_grn_drainage_systems.php, 2012.